Implementation and Comparative Study of Pyramid-based Image Fusion Techniques for Lumbar Spine Images

Manan M. Nanavati
Gujarat Technological University, India | Biomedical Engineering Department, Government Engineering College, India
manan.2507@gmail.com (corresponding author)

Mehul K. Shah
Instrumentation and Control Department, Vishwakarma Government Engineering College, India
mkshah2000@yahoo.com

Received: 14 April 2023 | Revised: 2 May 2023 | Accepted: 10 May 2023

 DOI: https://doi.org/10.48084/etasr.5960

ABSTRACT

Image fusion is a method of combining the necessary and relevant information from the set of source images into a single (fused) image which can be deemed to be more informative than the source. This paper discusses the implementation of various pyramid-based image fusion algorithms, such as the Laplacian pyramid, the ratio of the low-pass pyramid, the contrast pyramid, and the filter subtract decimate pyramid on multimodal CT and MR images of the lumbar spine. The fused images were evaluated using various objective evaluation quality metrics. The experimental results demonstrated that the ratio of the low pass pyramid achieved better performance compared to the other pyramids implemented, indicating that the fused image can also be used for further image fusion application or analysis purposes.

Keywords-lumbar spine; medical image fusion; objective evaluation criteria; pyramid transform

I. INTRODUCTION

Research in medical image processing is rapidly evolving and notable studies have been conducted in the last two decades. The main steps in medical image processing involve the acquisition of the biomedical signal, the formation of the image from the acquired biomedical signal, the processing of the image, and the display of the image for diagnosis. The devices for acquiring medical images consist of hardware and software elements. There are various sensors, such as radiography, Magnetic Resonance Imaging (MRI), Computed Tomography (CT), ultrasound (US), thermography, and nuclear medicine, that are widely used by clinicians and have attracted the interest of the researchers working in the area of medical imaging [1]. X-ray and CT are suitable and widely used for stationary images or images of hard tissues. MRI images are suitable for the examination of soft tissues, whereas Single Photon Emission CT (SPECT) and Positron Emission Tomography (PET) are nuclear imaging methods that provide details about organ metabolism [2]. CT and MRI are widely used for diagnostic or screening purposes, CT scans use an array of X-ray sensors to provide information about bony structures or hard tissues, and MRI uses a magnetic field to provide information on soft tissues, organs, and blood vessels. None of these imaging modalities can provide all the required details in one image. Hence, the fusion of data acquired from multiple sensors is necessary to get all the necessary information in one representative image. Medical image fusion combines data from different imaging sensors and merges the complementary information into a single representative image that can be used for better diagnosis and treatment. The main goal of medical image fusion is to conserve the necessary structures and information for improving clinical diagnosis and treatment planning.

Image fusion methods are broadly classified into three different types: pixel-level, feature-level, and decision-level [3]. Pixel-level fusion directly uses the values of pixel information from the source images to perform image fusion. The pixel-level method is more robust, fast, and easy to implement compared to the other two methods, as it can be implemented in both the spectral domain as well as in the transform domain, where the value and attributes of a given pixel are directly processed to attain the desired fusion result [4]. Methods like simple average, maximum or minimum selection, Principal Component Analysis (PCA) [4], Intensity Hue Saturation (IHS) [5], and Brovey transform [6] fall under the category of spatial domain techniques. The majority of the spatial domain techniques suffer from the drawback that they create spatial distortions in the output fused image which eventually leads to reduced spectral details. In most cases, this drawback is addressed by transform domain methods [7].

Feature-level fusion involves the fusion of features of the image, such as the intensity of pixels, edges, and textures, that are obtained by segmenting the source image as per the desired feature that needs to be fused. Decision-level fusion is a high-level fusion method that uses statistics, prediction, fuzzy logic heuristics, etc. The pixel level method is preferred in the majority of image fusion applications, as it can preserve the pixel values, is time efficient, and its implementation is easier compared to the other two methods.

Several different image fusion methods have been proposed [8-10]. In [11], an image fusion method based on Discrete Wavelet Transform (DWT) was proposed for medical images. In [12], a novel algorithm based on the quaternion Discrete Fourier Transform (DFT) for the multi-modal color image fusion of PET and CT images using the weighted fusion rule was proposed. In this method, the source image was first converted into a block and then into its quaternion form, and the fusion coefficients were computed using transform blocks by comparing the contrast value of subsequent coefficients. In [13], multi-resolution image fusion of MR and CT images based on DWT and Ripplet transform was proposed. In [14], image fusion of MR and PET images was performed using Hilbert Transform (HT) with Fourier Transform (FT) and HIS, but no evaluation method or criteria were mentioned for the output fused images. In [15], image fusion on PET and CT images was performed using eight different types of discrete wavelets, such as Haar, Daubechies (Db), Symlets (sym), Coiets (coif), discrete approximation of Meyer wavelet (Dmey), Biorthogonal (bior), Reverse biorthogonal (bior), and Fejer-Korovkin filters (fk). In [16], an image fusion method on PET and MRI images was proposed using DWT without loss of anatomical information on MRI images and minimum color distortion on PET images, pre-processing them with Gaussian filters. In [17], image fusion of CT and MRI images using a guided filter was proposed. In [18], another transform domain method for fusion was proposed, based on Hadamard transform and HVS. The computational complexity and blurring of the output fused images were overcome by Stationary Wavelet Transform (SWT) [19]. The source image was decomposed into HF and LF coefficients using SWT, and the maximum select rule was used for fusing HF and LF coefficients.

The averaging method is one of the simplest methods for image fusion, which uses the average of pixels from two or more source images. The main drawback of this method is that it is unable to produce clear objects or structures in the fused image. The simple maximum method selects the respective maximum value of the pixel from the input images. Its advantage is that it produces a high-focused image, but at the same time, the fused image suffers from a blurring effect that disturbs the local contrast. The FT method integrates the information concerning time, which results in a loss of information that varies with time in the fused image. The limitation of the quaternion FT approach is that it applies to color images such as PET and SPECT. In the case of image fusion using the guided filter, the pixel method performs better near edges rather than the whole image [20]. HT is very complex to understand and interpret when the source image has a very wide band frequency range, which is decomposed into its respective HF and LF coefficients. The Ripplet transform has more computational requirements than other basic transform domain methods. The main drawback of the Gaussian filter is that it loses the edge information, as it is mainly used in image smoothening. The DCT method produces real value coefficients, even in the case of input information being an integer, hence, a step of quantization to convert the real value number into an integer is required. The degradation of spectral data is the major drawback of the PCA method. Similarly to the quaternion approach, IHS is mainly applied to color images. There are also various advanced methods based on convolution neural networks for image fusion, but the only limitation is that they work only when the ground truth is available.

Various multiscale transform methods, such as the Laplacian pyramid, the ratio of low-pass pyramid, gradient pyramid, contrast pyramid, and DWT, have been proposed for image fusion. The conventional Wavelet Transform (WT) considers the local features of two images and the maximum absolute value of wavelet coefficients. Wavelets are found to be effective in representing objects with isolated point singularities but fail to represent objects with line singularities. Therefore, the methods based on WT or DWT are not able to preserve the edge quality and information from the source image to the output fused image. Considering all these constraints, this study implemented various pyramid transform methods, as they have the advantage of preserving global and local information in the spatial domain.

II. IMAGE FUSION USING PYRAMID TRANSFORM

An image pyramid [21] usually contains the band pass or low copies of an image and can also be described as the representation of source images by dividing them progressively into smaller and low-resolution sub-images. At every fusion level of the pyramid, the corresponding pyramid has half the size of the previous level pyramid. The basic concept of image fusion using pyramid transform is to obtain the pyramid transform of the fused image from the source image and eventually perform inverse pyramid transform. The pyramid transformation consists of the following major steps:

- Decomposition
- Initial image formation
- Recomposition

Decomposition is the process of generating the pyramid at each consecutive level of fusion. In general, the level of decomposition is predecided before performing the fusion and depends on various factors and the desired results. The decomposition process is performed l times, where l is the number of levels, and consists of the following steps:

- Low pass filtering: Various pyramid methods have their pre-defined filter to be used on the source or input images.
- Forming the pyramid from the filtered or convolved images using Burt's or Li's method.
- Decimate the input images to their half size and consider them as input for the next level of decomposition.

Initial image formation is performed by merging the input images after the process of decomposition. The resultant matrix of the image is considered as the input data of the recomposition process. Recomposition is a process in which the resultant image is formed from the pyramids at each level of decomposition. The recomposition process is performed l times, where l is the number of levels, and consists of the following steps:

- The input image is undecimated to the level of recomposition.
- The undecimated matrix of the image is further filtered or convolved with the transposition of the filter vector used in the decomposition.
- The filtered matrix is then further merged by the respective image fusion rules.
- The newly formed image matrix will be considered as the input to the next level of recomposition.
- The merged image at the final level of recomposition will be the final resultant fused image.

Different pyramids have different approaches to the decomposition and recomposition processes. The pyramids implemented in this study are described below. It would be better to understand the Gaussian pyramid method before implementing any other pyramid method. The Gaussian pyramid consists of low-pass filtered and downsampled images of the preceding level of the pyramid, where the base or first level is the source image, and creates a set of images by weighing down using the Gaussian average and further scaling down. Implementing it multiple times creates a stack of successive smaller images, where each pixel contains the local level information that corresponds to the neighborhood information on the lower level of the pyramid.

A. Filter Substract Decimate (FSD) Pyramid

The FSD pyramid is a computationally more efficient version of the Gaussian pyramid. As per the name of the pyramid, the image fusion using the FSD pyramid consists basically of the following steps:

1. Selection source image pair for fusion.
2. Selecting low-pass filtering using the filter mask $W = [\frac{1}{16}, \frac{4}{16}, \frac{6}{16}, \frac{4}{16}, \frac{1}{16}]$.
3. Selecting the level of fusion, i.e. decomposition level or recomposition level l.
4. The source images are filtered horizontally and vertically with the filter mask W.
5. The difference matrix is computed by subtracting the low-pass filtered images.
6. A pyramid is formed for the corresponding decomposition level using the select maximum or Burt's method or Li's method.
7. The formed pyramid is retained for the corresponding level l.
8. The images are decimated into half the size and steps 4 to 6 are repeated l times.
9. The final decimated pair named X image is processed using any of the following mathematical functions:
   a) Average
   b) Selection of Maximum
   c) Selection of Minimum
10. The matrix X obtained in the above step is undecimated with alternative zero padding of rows and columns.
11. The undecimated matrix is filtered or convolved with the doubly scaled filter mask W.
12. The filtered matrix is added to the retained level of the pyramid.
13. The matrix generated in step 12 acts as an input matrix X for the next level of recomposition.
14. The recomposition steps, i.e. steps 10-13, are repeated l times, which undecimates the matrices of each level and leads to the final fused image with the same size as the input source image.

The decomposition process takes steps 4-6, and the recomposition process takes steps 10-13.

B. Laplacian Pyramid

The Laplacian pyramid of a particular image is a set of bandpass images where each is a bandpass copy of its predecessor. The bandpass copy of the particular image can be computed by taking the difference between two low-pass images at successive levels of the Gaussian pyramid. The Laplacian pyramid is identical to the FSD pyramid, but in the decomposition phase, the additional filtering is performed with a $2\times W$ filter mask.

C. Ratio of Low Pass Pyramid

In the ratio of low-pass pyramid, every level of the image is the ratio of two successive levels of the Gaussian pyramid. It is also identical to the FSD pyramid, where in the decomposition step the pixel-wise ratio is taken rather than the subtraction as in the FSD pyramid method.

D. Gradient Pyramid

The gradient pyramid is almost similar to the FSD pyramid with only the change of the filter mask and the additional directional filter implemented in the decomposition step. The filter mask uses $W = [\frac{1}{16}, \frac{4}{16}, \frac{6}{16}, \frac{4}{16}, \frac{1}{16}]$ and $V = [\frac{1}{4}, \frac{2}{4}, \frac{1}{4}]$. The directional filter masks implemented are the Horizontal filter mask (H), the Vertical filter mask (V), and the Diagonal filter masks ($D1$ and $D2$), respectively. The rest steps are similar to the FSD pyramid.

$$H = \begin{bmatrix} 0 & 0 & 0 \\ 1 & -2 & 1 \\ 0 & 0 & 0 \end{bmatrix}$$

$$V = \begin{bmatrix} 0 & 1 & 0 \\ 0 & -2 & 0 \\ 0 & 1 & 0 \end{bmatrix}$$

$$D1 = \begin{bmatrix} 0 & 0 & 0.5 \\ 0 & -1 & 0 \\ 0.5 & 0 & 0 \end{bmatrix}$$

$$D2 = \begin{bmatrix} 0.5 & 0 & 0 \\ 0 & -1 & 0 \\ 0 & 0 & 0.5 \end{bmatrix}$$

E. Contrast Pyramid

The contrast pyramid is similar to the ratio of low-pass pyramid but takes the ratio of the difference between luminescence and local background luminescence. Luminescence is a measure of brightness and the amount of visible light leaving a particular surface area.

III. METHODOLOGY AND EXPERIMENTAL SETUP

A. Methodology

As discussed above, the main goal of image fusion is to combine two or more images and their information to produce a resultant single image that contains information from all the source images. Image fusion basically involves three major steps: image registration, image pre-processing, and applying an image fusion algorithm. Image registration is a process that involves overlaying or aligning two or more images that are recorded from different angles, different points, different distances, or different time instances by considering one image as a reference or fixed image [22]. The main purpose of registering an image before image fusion is to geometrically align two images generated from different sensors. As the image is generated through different sensors of the same body part and from different viewpoints, the image fusion process is not possible unless the two images are geometrically aligned with each other.

In this study, the intrinsic approach based on landmarks, also known as control point mapping, was used as a method to register the source CT and MR images, as the dataset used contained very few pairs of images. The registration method requires users to manually select the landmark/control points in the source images. Once the positions of the landmark points are obtained, geometric transformations like affine, projective, or polynomial geometric transforms are applied to the source images. One of the main advantages of the landmark-based image registration method is that it focuses on the specific features/points selected by the user rather than automatically registering the image based on all the features. This study performed spine fusion using landmark or focus areas of disc alignment, disc degeneration, and vertebrae(s). The major steps involved in image registration using landmark points are:

1. Selecting the moving and the fixed image from a pair of source images.
2. Manually selecting the landmark points.
3. Fine-tuning the selected landmark points.
4. Select the appropriate transform to apply to the source image, considering the selected points to obtain the registered image.

The pre-processing stage mainly involves brightness and contrast matching of source CT and MR images to lose the least level of information. The main purpose of pre-processing is to match the level of contrast for a better fusion outcome, and it was also performed due to the source image taken from different sensors at different angles or heights. The pyramids discussed in the previous section were implemented to evaluate their image fusion performance. The level of decomposition was kept at 4 in all experiments. The low-frequency components were fused with the average rule, which takes the average of the absolute pyramid coefficient at each location from the input images as the coefficient at that location in the fused image.

The main steps for the image fusion using pyramid-based transform are as follows:

- Step 1: Image registration of the source images, so that the corresponding pixel or region of the image is aligned geometrically with each other.
- Step 2: Application of pyramid transforms on the input images to get the decomposed images. The transformed image contains various levels of selected pyramids.
- Step 3: The appropriate fusion rule is applied for merging the pyramid levels of the source image.
- Step 4: The recomposition of the merged pyramid level was performed by applying inverse pyramid transform to produce the resultant fused image.

Figure 1 shows a schematic flow chart of the implemented pyramid transform-based approach. The goal of image fusion is to preserve maximum information, such as edges and textures, from the source images. In any image, the necessary and important features are generally larger than a pixel, and the conventional pixel-by-pixel fusion may not preserve the necessary information from the source image. For the fusion of high-pass coefficients, the max select rule with consistency check proposed in [23] was used, which effectively checks that the dominant features are incorporated into the fused image.

B. Experimental Setup

The source images were registered CT and MRI T1 images of the lumbar spine with dimensions of 512×512. SpineWeb dataset 1 was used, which contains 17 pairs of multimodal CT and MR images [24]. The landmark-based method for image registration and pyramid transforms for image fusion was used, with a decomposition level of 4. The experiments were carried out in a Ryzen 7 3.3GHz, 16GB DDR4 RAM, 6GB NVIDIA Graphics Memory PC, and MATLAB v. 2021a.

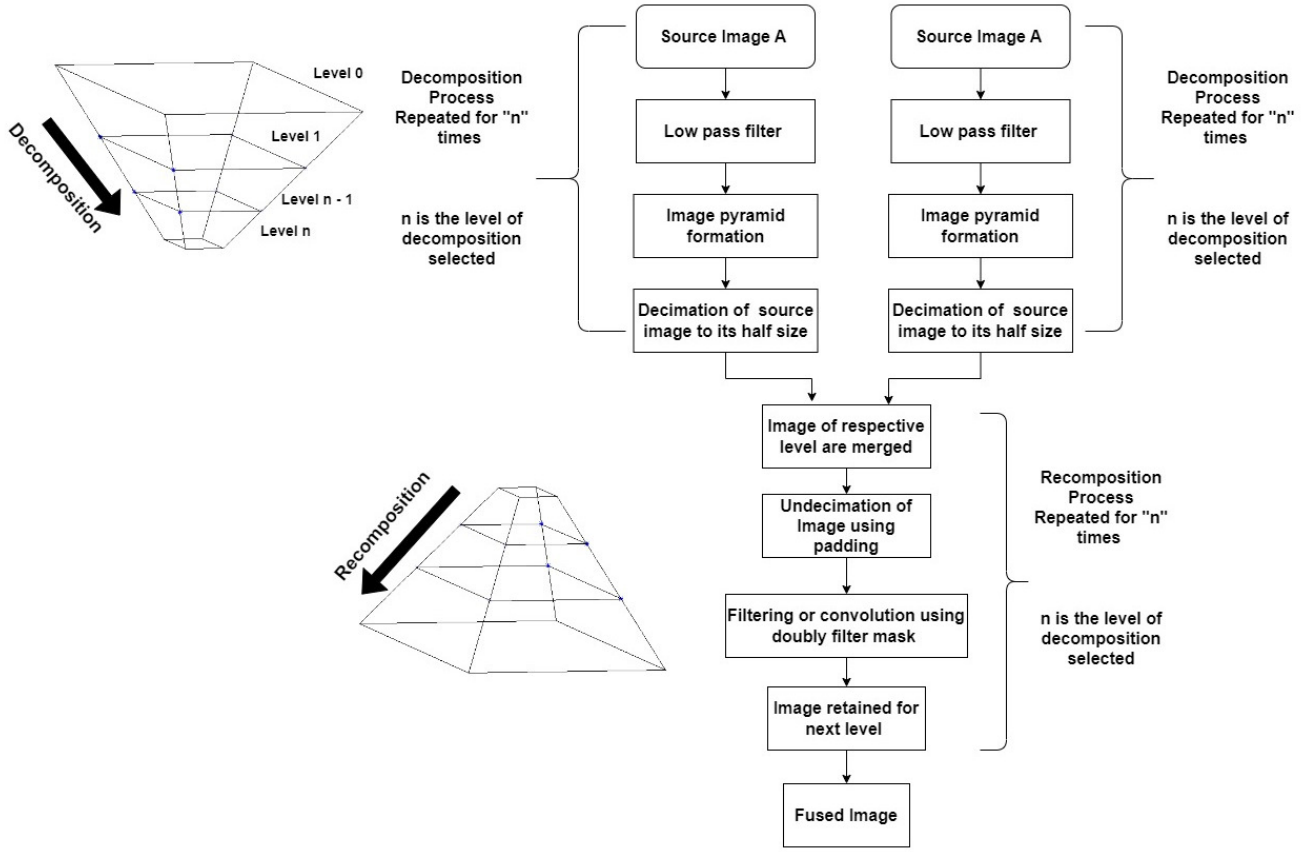

Fig. 1. Block diagram of image fusion based on pyramid-based transform.

IV. OBJECTIVE EVALUATION METRICS

It is tough to evaluate the quality of the fused image when the reference image or ground truth is not available for comparison. In the past decade, many metrics have been proposed to compute quality, but none of them is universally accepted as a gold standard evaluation metric. Hence, it is necessary to evaluate various metrics to summarize any study. This study analyzed the objective assessment following several quality metrics: Spatial frequency, entropy (E) [25], mutual information (MI) [26], $Q^{AB/F}$ [27], Q^{MI} [28], and Q^{TE} [29].

V. RESULT ANALYSIS

For experimental analysis, various pyramid-based fusion algorithms were implemented and applied to the SpineWeb dataset 1. Due to space limitation, only 4 cases are demonstrated here in the form of tables, out of which 2 cases are demonstrated with images. The outcomes of all pyramid-based fusion algorithms were evaluated using the quality metrics described above. Figure 2 represents the source image of CT and MR for the 2 cases, while Figures 3 and 4 show the output of the implemented fusion algorithms. Table I shows the values of the quality metrics of the fused images of the two cases presented in Figure 3 and Figure 4, while Table II shows the quality metrics values for images not presented in this paper, but whose quality parameters are discussed. The best value of each quality metric is highlighted for every case. It is observed that the ratio of the low pass pyramid and the Laplacian pyramid has consistently shown the best results in all four cases discussed.

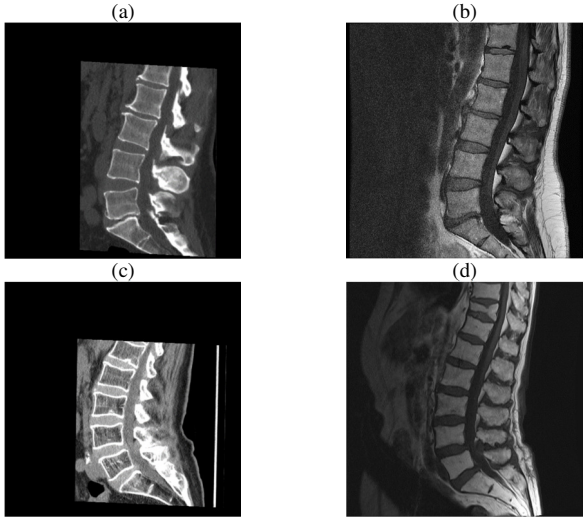

Fig. 2. (a), (b) Registered source image of CT and MR for Case–1, (c), (d) Registered source image of CT and MR for Case–2.

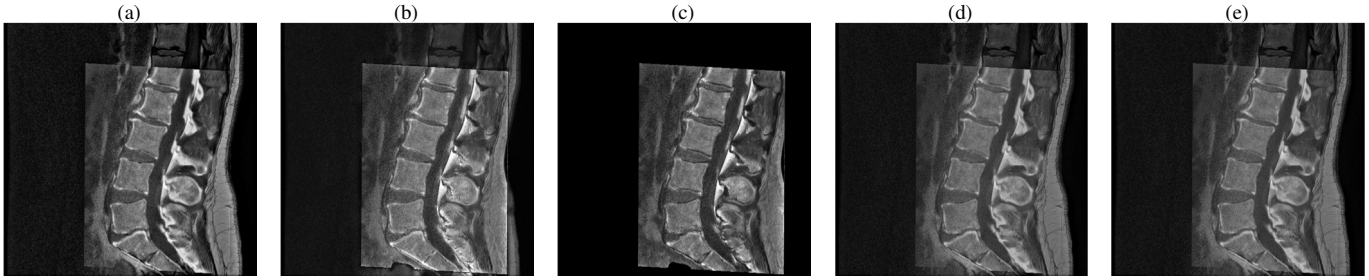

Fig. 3. Output fused image of Case–1 using: (a) Laplacian pyramid, (b) ratio of low pass pyramid, (c) contrast pyramid, (d) FSD pyramid, (e) gradient pyramid.

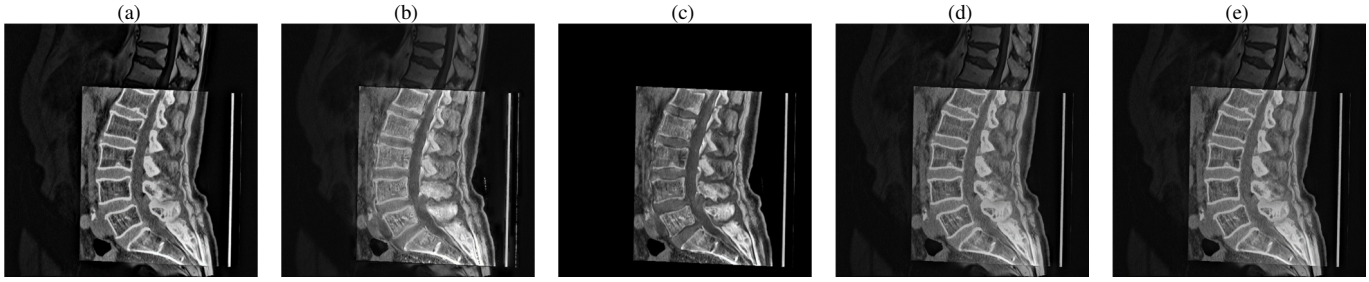

Fig. 4. Output fused image of Case–2 using: (a) Laplacian pyramid, (b) ratio of low pass pyramid, (c) contrast pyramid, (d) FSD pyramid, (e) gradient pyramid.

TABLE I. QUALITY METRICS FOR CASES 1 AND 2

Case	Pyramid type	*SF*	*E*	*MI*	$Q^{AB/F}$	Q^{MI}	Q^{TE}
1	Laplacian	15.3038	**7.0184**	2.7677	**0.7011**	0.4314	0.4314
	RLP	**17.0576**	6.9415	**3.7702**	0.4640	**0.5807**	**0.5807**
	Contrast	14.8091	4.2662	2.0214	0.2278	0.4352	0.4352
	FSD	12.0528	6.9588	3.1003	0.6464	0.4852	0.4852
	Gradient	11.9134	6.9444	3.1252	0.6479	0.4892	0.4892
2	Laplacian	18.7665	**6.7103**	2.4883	**0.7071**	0.4328	0.4096
	RLP	**19.2908**	6.6277	**3.2522**	0.4332	**0.5508**	**0.4795**
	Contrast	16.4682	3.5317	1.7548	0.2050	0.4606	0.3925
	FSD	14.7722	6.5286	2.9068	0.6288	0.5097	0.4712
	Gradient	14.6945	6.5283	2.9203	0.6322	0.5116	0.4723

TABLE II. QUALITY METRICS FOR CASES 3 AND 4

Case	Pyramid type	*SF*	*E*	*MI*	$Q^{AB/F}$	Q^{MI}	Q^{TE}
3	Laplacian	15.7928	**6.5974**	2.6297	**0.7226**	0.4581	0.4329
	RLP	**16.7283**	6.4760	**3.8602**	0.4429	**0.6530**	**0.5168**
	Contrast	15.3242	3.2962	1.7120	0.1930	0.4788	0.3916
	FSD	13.0246	6.4243	3.1716	0.6510	0.5568	0.5061
	Gradient	12.9487	6.4253	3.1954	0.6543	0.5606	0.5072
4	Laplacian	15.2186	**6.6256**	2.4380	**0.6826**	0.4212	0.3936
	RLP	**17.2562**	6.5498	**3.1009**	0.3791	**0.5271**	**0.4944**
	Contrast	15.5048	4.2799	2.0556	0.1638	0.4661	0.4163
	FSD	12.2355	6.4844	2.9927	0.6154	0.5228	0.4809
	Gradient	12.1843	6.4821	3.0121	0.6187	0.5262	0.4923

Mutual Information (*MI*) indicates the amount of information from the source image that is retained in the fused image. The ratio of the low-pass pyramid has shown the highest value for *MI* in all the cases presented in this study compared to the other pyramid algorithms. The highest value in metrics such as *SF*, Q^{MI}, and Q^{TE}, where a higher *SF* value means that the output fused image is of good quality and Q^{MI} and Q^{TE} are information theory-based metrics, indicates that in the fused image, more information can be extracted from the source image. The value of Entropy (*E*) and $Q^{AB/F}$ was consistently higher in all four cases for the Laplacian pyramid. Higher values of Entropy indicate the presence of more information in the fused image and higher values of $Q^{AB/F}$ indicate that the Laplacian pyramid method was able to preserve more edge information from the source image compared to the other pyramid-based methods. The spatial frequency value obtained for the FSD and gradient pyramid is the lowest, indicating the overall poor quality of the output fused images compared to the other pyramids. The Entropy value and *MI* of the contrast pyramid method were low compared to the others, which indicates less information is present in the output fused images.

Comparing the values of Entropy of the fused image in Tables I and II for the Laplacian pyramid and the ratio of the low-pass pyramid, it was observed that there is no significant difference between. Considering all the metric values obtained, the ratio of the low-pass pyramid performed well in all cases compared to the other pyramid-based algorithms.

VI. SUMMARY

This study implemented various pyramid-based image fusion algorithms on MRI and CT images of the lumbar spine. The performance of the implemented algorithms was analyzed by measuring various quality metrics of the fused image. The experiments demonstrated that the ratio of the low-pass pyramid achieved comparable performance in terms of quality metrics compared to its counterpart pyramids implemented. The main goal of image fusion is to increase the accuracy of diagnosis and assist clinicians in decision-making. Several studies have developed automated decision support systems based image features [30-31]. In the future, this study can be

extended to implement various image fusion algorithms on a large multimodal dataset of the spine to develop a decision support system.

REFERENCES

[1] R. Jha and T. Singh, "Multinomial logistic regression for breast thermogram classification," in *2017 International Conference on Communication and Signal Processing (ICCSP)*, Chennai, India, Apr. 2017, pp. 1266–1271, https://doi.org/10.1109/ICCSP.2017.8286584.

[2] H. K. Huang, "Biomedical image processing," *Critical reviews in bioengineering*, vol. 5, no. 3, pp. 185–271, Jan. 1981.

[3] Y. Yang *et al.*, "Multi-Focus Image Fusion via Clustering PCA Based Joint Dictionary Learning," *IEEE Access*, vol. 5, pp. 16985–16997, 2017, https://doi.org/10.1109/ACCESS.2017.2741500.

[4] H. M. El-Hoseny, W. Abd Elrahman, E. S. M. El. Rabaie, O. S. Faragallah, and F. E. Abd El-Sami, "Medical Image Fusion: A Literature Review Present Solutions and Future Directions," *Menoufia Journal of Electronic Engineering Research*, vol. 26, no. 2, pp. 321–350, Jul. 2017, https://doi.org/10.21608/mjeer.2017.63510.

[5] W. Kong, Y. Lei, and X. Ni, "Fusion technique for grey-scale visible light and infrared images based on non-subsampled contourlet transform and intensity–hue–saturation transform," *IET Signal Processing*, vol. 5, no. 1, pp. 75–80, Feb. 2011, https://doi.org/10.1049/iet-spr.2009.0263.

[6] R. A. Mandhare, P. Upadhyay, and S. Gupta, "Pixel-Level Image Fusion Using Brovey Transforme and Wavelet Transform," *International Journal of Advanced Research in Electrical, Electronics and Instrumentation Engineering*, vol. 2, no. 6, Jun. 2013.

[7] V. P. S. Naidu and J. R. Raol, "Pixel-level Image Fusion using Wavelets and Principal Component Analysis," *Defence Science Journal*, vol. 58, no. 3, Mar. 2008, https://doi.org/10.14429/dsj.58.1653.

[8] S. Li, X. Kang, L. Fang, J. Hu, and H. Yin, "Pixel-level image fusion: A survey of the state of the art," *Information Fusion*, vol. 33, pp. 100–112, Jan. 2017, https://doi.org/10.1016/j.inffus.2016.05.004.

[9] F. E. Z. A. El-Gamal, M. Elmogy, and A. Atwan, "Current trends in medical image registration and fusion," *Egyptian Informatics Journal*, vol. 17, no. 1, pp. 99–124, Mar. 2016, https://doi.org/10.1016/j.eij.2015.09.002.

[10] A. P. James and B. V. Dasarathy, "Medical image fusion: A survey of the state of the art," *Information Fusion*, vol. 19, pp. 4–19, Sep. 2014, https://doi.org/10.1016/j.inffus.2013.12.002.

[11] S. Cheng, J. He, and Z. Lv, "Medical Image of PET/CT Weighted Fusion Based on Wavelet Transform," in *2008 2nd International Conference on Bioinformatics and Biomedical Engineering*, Shanghai, China, Feb. 2008, pp. 2523–2525, https://doi.org/10.1109/ICBBE.2008.964.

[12] Q. Nawaz, B. Xiao, I. Hamid, and D. Jiao, "Multi-modal Color Medical Image Fusion Using Quaternion Discrete Fourier Transform," *Sensing and Imaging*, vol. 17, no. 1, Apr. 2016, Art. no. 7, https://doi.org/10.1007/s11220-016-0131-x.

[13] C. T. Kavitha, C. Chellamuthu, and R. Rajesh, "Medical Image Fusion using Combined Discrete Wavelet and Ripplet Transforms," *Procedia Engineering*, vol. 38, pp. 813–820, Jan. 2012, https://doi.org/10.1016/j.proeng.2012.06.102.

[14] M. Haddadpour, S. Daneshvar, and H. Seyedarabi, "PET and MRI image fusion based on combination of 2-D Hilbert transform and IHS method," *Biomedical Journal*, vol. 40, no. 4, pp. 219–225, Aug. 2017, https://doi.org/10.1016/j.bj.2017.05.002.

[15] A. R. Doke, T. Singh, K. Shantanu, and R. Nayar, "Comparative analysis of wavelet transform methods for fusion of CT and PET images," in *2017 IEEE International Conference on Power, Control, Signals and Instrumentation Engineering (ICPCSI)*, Chennai, India, Sep. 2017, pp. 2152–2156, https://doi.org/10.1109/ICPCSI.2017.8392098.

[16] Bhavana V. and Krishnappa H.K., "Multi-Modality Medical Image Fusion using Discrete Wavelet Transform," *Procedia Computer Science*, vol. 70, pp. 625–631, Jan. 2015, https://doi.org/10.1016/j.procs.2015.10.057.

[17] Y. Na, L. Zhao, Y. Yang, and M. Ren, "Guided filter-based images fusion algorithm for CT and MRI medical images," *IET Image Processing*, vol. 12, no. 1, pp. 138–148, 2018, https://doi.org/10.1049/iet-ipr.2016.0920.

[18] R. Vadhi, V. S. Kilari, and S. S. Kumar, "An Image Fusion Technique Based on Hadamard Transform and HVS," *Engineering, Technology & Applied Science Research*, vol. 6, no. 4, pp. 1075–1079, Aug. 2016, https://doi.org/10.48084/etasr.707.

[19] O. Prakash and A. Khare, "CT and MR Images Fusion Based on Stationary Wavelet Transform by Modulus Maxima," in *Computational Vision and Robotics*, New Delhi, India, 2015, pp. 199–204, https://doi.org/10.1007/978-81-322-2196-8_23.

[20] A. Gadge and D. S. S. Agrawal, "Guided Filter for Color Image," International Journal of Innovative Research in Electrical, Electronics, Instrumentation and Control Engineering, vol. 4, no. 6, pp. 250–252, Jun. 2016.

[21] J. J. Lewis, R. J. O'Callaghan, S. G. Nikolov, D. R. Bull, and N. Canagarajah, "Pixel- and region-based image fusion with complex wavelets," *Information Fusion*, vol. 8, no. 2, pp. 119–130, Apr. 2007, https://doi.org/10.1016/j.inffus.2005.09.006.

[22] B. Zitová and J. Flusser, "Image registration methods: a survey," *Image and Vision Computing*, vol. 21, no. 11, pp. 977–1000, Oct. 2003, https://doi.org/10.1016/S0262-8856(03)00137-9.

[23] H. Li, B. S. Manjunath, and S. K. Mitra, "Multisensor Image Fusion Using the Wavelet Transform," *Graphical Models and Image Processing*, vol. 57, no. 3, pp. 235–245, May 1995, https://doi.org/10.1006/gmip.1995.1022.

[24] "Spineweb online database." http://spineweb.digitalimaginggroup.ca/.

[25] R. Nair, T. Singh, and R. Nayar, "Logistic regression for Mouth (orotracheal) or Nose (nasotracheal) endotracheal intubation," in *2017 IEEE International Conference on Power, Control, Signals and Instrumentation Engineering (ICPCSI)*, Chennai, India, Sep. 2017, pp. 2026–2031, https://doi.org/10.1109/ICPCSI.2017.8392071.

[26] C. S. Xydeas and V. Petrović, "Objective image fusion performance measure," *Electronics Letters*, vol. 36, no. 4, pp. 308–309, Feb. 2000, https://doi.org/10.1049/el:20000267.

[27] S. Li, B. Yang, and J. Hu, "Performance comparison of different multi-resolution transforms for image fusion," *Information Fusion*, vol. 12, no. 2, pp. 74–84, Apr. 2011, https://doi.org/10.1016/j.inffus.2010.03.002.

[28] M. Hossny, S. Nahavandi, and D. Creighton, "Comments on 'Information measure for performance of image fusion,'" *Electronics Letters*, vol. 44, no. 18, pp. 1066–1067, Aug. 2008, https://doi.org/10.1049/el:20081754.

[29] N. Cvejic, C. Canagarajah, and D. Bull, "Image fusion metric based on mutual information and tsallis entropy," *Electronics Letters*, vol. 42, no. 11, pp. 626–627, May 2006, https://doi.org/10.1049/iel:20060693.

[30] N. Behar and M. Shrivastava, "A Novel Model for Breast Cancer Detection and Classification," *Engineering, Technology & Applied Science Research*, vol. 12, no. 6, pp. 9496–9502, Dec. 2022, https://doi.org/10.48084/etasr.5115.

[31] N. Kumar, A. Hashmi, M. Gupta, and A. Kundu, "Automatic Diagnosis of Covid-19 Related Pneumonia from CXR and CT-Scan Images," *Engineering, Technology & Applied Science Research*, vol. 12, no. 1, pp. 7993–7997, Feb. 2022, https://doi.org/10.48084/etasr.4613.